



Publication Year	2016
Acceptance in OA	2020-04-30T12:24:22Z
Title	The SpaceInn-SISMA Database: Characterization of a Large Sample of Variable and Active Stars by Means of HARPS Spectra
Authors	RAINER, Monica, PORETTI, Ennio, MISTO', Angelo, PANZERA, Maria Rosa, MOLINARO, Marco, CEPPARO, Francesco, Roth, M., Michel, E., Monteiro, M. J. P. F. G.
Publisher's version (DOI)	10.3847/0004-6256/152/6/207
Handle	http://hdl.handle.net/20.500.12386/24364
Journal	THE ASTRONOMICAL JOURNAL
Volume	152



THE SPACEINN–SISMA DATABASE: CHARACTERIZATION OF A LARGE SAMPLE OF VARIABLE AND ACTIVE STARS BY MEANS OF HARPS SPECTRA

M. RAINER¹, E. PORETTI¹, A. MISTÒ¹, M. R. PANZERA¹, M. MOLINARO², F. CEPparo², M. ROTH³,
E. MICHEL⁴, AND M. J. P. F. G. MONTEIRO⁵

¹ INAF-Osservatorio Astronomico di Brera, via E. Bianchi 46, I-23807 Merate, Italy; monica.rainer@brera.inaf.it

² INAF-Osservatorio Astronomico di Trieste, via Tiepolo 11, I-34143, Trieste, Italy

³ Kiepenheuer-Institut für Sonnenphysik, Schönebeckstr. 6, D-79104 Freiburg, Germany

⁴ Observatoire de Paris, LESIA, UMR8109, Université Pierre et Marie Curie, Université Paris Diderot, PSL, 5 pl. J. Jassen, F-92195 Meudon, France

⁵ Instituto de Astrofísica e Ciências do Espaço, CAUP & DFA/FCUP, Universidade do Porto, Rua das Estrelas, 4150-762 Porto, Portugal

Received 2016 September 15; revised 2016 November 7; accepted 2016 November 7; published 2016 December 5

ABSTRACT

We created a large database of physical parameters and variability indicators by fully reducing and analyzing the large number of spectra taken to complement the asteroseismic observations of the *CONvection, ROTation and planetary Transits (CoRoT)* satellite. 7103 spectra of 261 stars obtained with the ESO echelle spectrograph HARPS have been stored in the VO-compliant database *Spectroscopic Indicators in a SeisMic Archive (SISMA)*, along with the *CoRoT* photometric data of the 72 *CoRoT* asteroseismic targets. The remaining stars belong to the same variable classes of the *CoRoT* targets and were observed to better characterize the properties of such classes. Several useful variability indicators (mean line profiles, indices of differential rotation, activity and emission lines) together with $v \sin i$ and radial-velocity measurements have been extracted from the spectra. The atmospheric parameters T_{eff} , $\log g$, and $[\text{Fe}/\text{H}]$ have been computed following a homogeneous procedure. As a result, we fully characterize a sample of new and known variable stars by computing several spectroscopic indicators, also providing some cases of simultaneous photometry and spectroscopy.

Key words: asteroseismology – astronomical databases: miscellaneous – line: profiles – stars: fundamental parameters – stars: variables: general

Supporting material: machine-readable table

1. INTRODUCTION

The huge amount of stars observed from space needs for an intensive, time-consuming, ground-based follow-up to confirm both the correct identification of the source and its full characterization. This issue will rapidly grow in the future, since new all-sky missions are ready to be launched or are in advanced drawing. Therefore, it is of paramount importance to store the data and the information in a way that they can be exploited in the future to drive, complement, and help the new analyses, making the incoming ground-based follow-ups more robust and straightforward.

In this context the ground-based activities performed in support of the *CONvection, ROTation and planetary Transits (CoRoT)*; Baglin et al. 2007) space mission are playing a relevant role. The two main scientific programs of the *CoRoT* mission focused on asteroseismic studies and an extrasolar planets search. Each program used two dedicated CCDs and had different observational strategies: the asteroseismic program observed up to 5 stars brighter than magnitude $m_V = 9$ per CCDs (10 in total) per observing run, while the exoplanet program observed around 6000 stars per CCD (12,000 in total) of magnitude between 11 and 16. *CoRoT* was launched on 2006 December 27 and it was retired on 2013 June 24 after a second, unrecoverable electronic failure occurred on 2012 November 2. The first failure, in 2009 March, caused the loss of two CCDs and the halving of the number of targets.

The whole asteroseismic program was flanked by a large ground-based observational effort ensuring a simultaneous monitoring (Poretti et al. 2007, 2013; Uytterhoeven et al. 2009; Rainer et al. 2012). Such a strategic decision was taken in the mission planning before launch in order to combine the high-

quality photometry with simultaneous high-resolution spectroscopy. The asteroseismic strategy of the space mission *CoRoT* was to monitor several different types of pulsating and variable stars in order to cover almost the whole Hertzsprung–Russell diagram (Table 1). The observations were carried out on alternating short and long observing runs, of about 30 and 150 days respectively, focusing on up to 10 stars per run before the first failure and to 5 stars afterwards.

The ground-based activities started with the Large Programme 178.D-0361 using the FEROS spectrograph at the 2.2 m telescope of the ESO-La Silla Observatory, and continued with the Large Programmes LP182.D-0356 and LP185.D-0056 using the HARPS instrument at the 3.6 m ESO telescope (Mayor et al. 2003). The spectroscopic survey branched out to several other high-resolution echelle spectrographs, i.e., SOPHIE at the Observatoire de Haute Provence, FOCES at Calar Alto Observatory, FIES and HERMES at the Roque de Los Muchachos Observatory, CORALIE at ESO-La Silla Observatory, and HERCULES at the Mount John University Observatory.

The need to make such a large archive of high-resolution spectra available to the whole community became urgent with the end of the *CoRoT* mission. Therefore, a specific activity was included in the *SpaceInn: Exploitation of Space Data for Innovative Helio- and Asteroseismology*⁶ project. One of the purposes of this project is to establish and coordinate archives of helio- and asteroseismic data, both new and already existing. Furthermore, the project aims to make public the results of the analysis of these data and the tools that have been developed in

⁶ <http://www.spaceinn.eu/>

Table 1
Type and Number of Variables in SISMA

Variable Type	Label	Number of Stars
Main Sequence Stars		
O-early-B stars	OB	8
Emission line B stars	Be	41
Slowly pulsating B-type stars	SPB	23
Slowly pulsating B-type stars- β Cephei hybrid	SPB-bCep	2
β Cephei	bCep	6
α^2 Canum Venaticorum	a2CVn	4
Chemically peculiar HgMn stars	HgMn	2
late B-A-F stars	BAF	13
δ Scuti	dSct	97
δ Scuti- γ Doradus hybrid	dSct-gDor	1
γ Doradus	gDor	22
T Tauri stars	TTau	1
Solar-like stars	solar-like	14
Evolved Stars		
α Cygni	aCyg	1
S Doradus	SDor	2
Red giants	red giant	23
RR Lyrae	RRLyr	1

treating them. As such, we pursued one of the *SpaceInn* goals by creating an archive to store not only the reduced spectra, but also a whole range of information on the variability content of the observed time series. In line with the project, we would like now to make the data accessible also to the broader scientific community beyond the *CoRoT* asteroseismic one.

Since HARPS was by far the most-used instrument in our observational program, first we focused on the 7135 spectra collected on 261 targets. Future activities, perhaps in other projects, could be the full reduction of the more diversified spectra collected with the other spectrographs. Thirty-two HARPS spectra have been discarded for quality reasons, and the remaining 7103 have been stored in the web-based VO-compliant archive *Spectroscopic Indicators in a SeisMic Archive* (SISMA), along with additional files and information. In this paper, we illustrate the work done collecting the spectra, reducing them, and obtaining the full set of spectroscopic indicators (physical parameters, velocities, activity indices, and so on) of stars belonging to several classes of variables.

2. OBSERVATIONS AND REDUCTION OF THE HARPS SPECTRA

In the framework of the awarded two HARPS Large Programmes, 15 nights were allocated each semester over nine semesters, from 2008 December to 2013 January, for a total of 135 nights. The HARPS spectrograph covers the spectral range from 3780 to 6910 Å, distributed over echelle orders 89–161. We usually used it in the high-efficiency mode EGGs, with resolving power $R = 80,000$ to obtain high signal-to-noise ratio (S/N) spectroscopic time series. Indeed, many of the *CoRoT* targets were hot stars, with large $v \sin i$ values, thus making the high-accuracy mode HAM ($R = 115,000$) ineffective in improving the radial-velocity precision. We also note that the library of masks used by the online reduction pipeline of HARPS does not include hot star templates, again lowering the precision of the radial-velocity measurements for hot stars, even in the case of low $v \sin i$ values. Moreover, the EGGs

mode allowed us also to reduce the exposure times, and to increase the S/N, which is very useful for the line-profile variations (LPVs) analysis. Nevertheless, some specific targets (cool, bright stars with low $v \sin i$) have been observed in the high-accuracy mode HAM, more appropriate for obtaining very precise radial-velocity measurements for these cases. The statistical mode of the S/N of the EGGs spectra is $S/N = 220$ at about 5800 Å, while that of the HAM spectra is $S/N = 160$ in the same region.

In addition to the primary targets, the satellite observed some specific asteroseismic targets in the exo CCDs, too. These objects are typically faint ($11 \leq m_V \leq 16$) and unsuitable for detailed spectroscopic studies. Nevertheless, we took a few spectra for some of them in order to obtain the physical parameters (e.g., Poretti et al. 2011). As requested in the case of observations conducted in Visitor Mode, other objects were observed as back-up and filling targets, aiming at better defining the physical properties of the variability classes observed by *CoRoT*.

All of the HARPS spectra were reduced using a semi-automated pipeline developed at the Brera Observatory (Rainer 2003), which automatically normalizes the spectra and retains information on the wavelength range of the orders (see Appendix A for more details on the reduction). The latter is very important for detailed spectroscopic analysis, because the S/N decreases greatly on the borders of the orders and the spectral lines in these regions may be distorted during the merging because of a lack of continuum on both sides of the lines. Our pipeline delivers two outputs for each spectrum: (a) a five-column table with wavelength, flux, normalized flux, S/N, and number of the echelle orders; (b) a two-column table with wavelength and normalized flux, with the echelle orders merged. The normalization was done in an automated way, as such, the normalized spectra are to be used with care, keeping in mind that the normalization could be unreliable in the first blue orders and on the borders of the orders.

We adopted a classification of the variable stars based on a preliminary analysis of the *CoRoT* light curves, HARPS spectra, and previous studies of the 261 targets (Table 1). In particular, several late B, A, and F stars selected as asteroseismic targets for *CoRoT* turned out to be constant or elusive variables. We grouped them under the “BAF stars” label. On the other hand, the O and early-B stars class seems more intriguing, since the interplay between pulsation and rotation is still unclear in these hot stars (Blomme et al. 2012). These targets, together with the calibration stars HD 34816 and HD 135240, are grouped under the “OB” label.

3. DATA ANALYSIS: INDICATORS

Our archive complements the in-depth papers devoted to particular asteroseismic *CoRoT* targets (e.g., Floquet et al. 2009; Poretti et al. 2009; Mantegazza et al. 2012; Escorza et al. 2016). For this purpose, we provide additional information on the objects that can help in this endeavour by adding some useful indicators, focusing on those that will help the study of stellar variability, caused either by pulsations, rotational activity, or emissions.

3.1. Mean Line Profiles: LPVs and Rotational Velocities

We computed the mean line profiles of each spectrum by means of the least-squares deconvolution (LSD) software

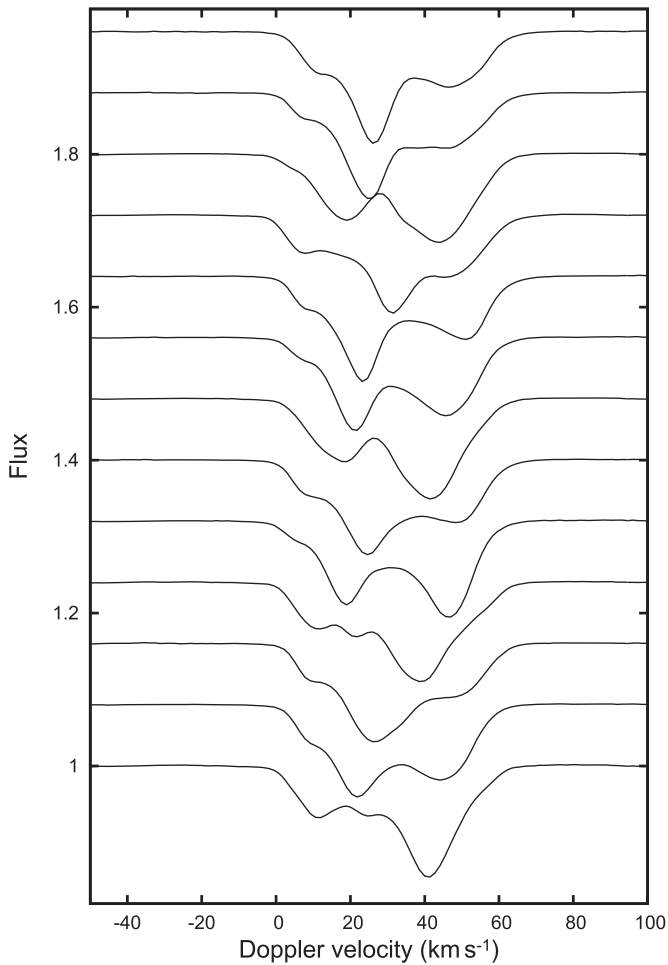


Figure 1. Mean line profiles of the δ Scuti star HD 41641 at intervals of about 25 min. The fluxes have been shifted for easier interpretation. The line-profile variations are greatly enhanced by averaging a great number of spectral lines.

(Donati et al. 1997). This method greatly enhances the S/N, allowing it to reach $S/N \gg 1000$ (e.g., Poretti et al. 2009; Mantegazza et al. 2012) since it grows roughly following \sqrt{N} , where N is the number of the used lines (see Figure 1 in Donati et al. 1997).

The LSD procedure requires as input normalized spectra and theoretical line masks (obtained from VALD, see Piskunov et al. 1995). The presence of saturated lines will greatly influence the shape of the resulting profiles, while telluric lines, which are not present in the mask, will increase the noise of the results. In order to obtain the best possible mean line profiles, we selected the wavelength regions 4415–4805, 4915–5285, and 5365–6505 Å; i.e., we cut (a) the blue end of the spectra (orders 139–161), where usually the S/N is very low and the automated normalization procedure may fail (see Appendix A); (b) the red end of the spectra (orders 89–93), where most of the telluric lines are found; and (c) the regions of the Balmer lines. We used a 0.8 km s^{-1} step for the HAM spectra and a 1.4 km s^{-1} step for the EGS spectra, aside from some cases where we were forced to compute the mean line profiles in a very large velocity range (up to 1000 km s^{-1}) to take into account very fast rotation in binaries, as such, we increased the step up to 4 km s^{-1} for computational reasons. The mean line profiles are extremely useful to give clues of the importance of the nonradial oscillations. Figure 1 shows the clear

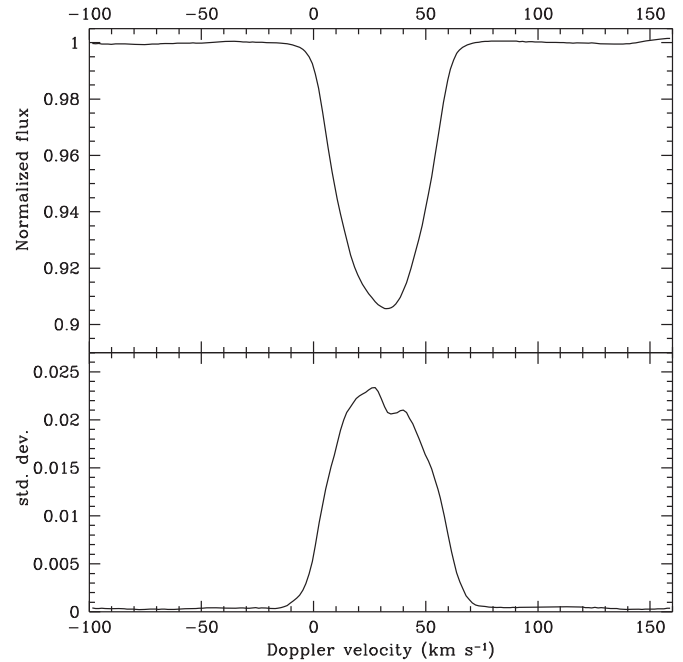


Figure 2. Average mean line profile and standard deviations for the δ Scuti star HD 41641. The line-profile variations are clearly concentrated at the center of the line.

perturbations due to a nonradial pressure mode in the mean line profiles of the δ Sct star HD 41641: the most probable identification of such a mode is $(\ell, m) = (3, 1)$ (Escorza et al. 2016). The LPVs also provide the most stringent piece of evidence that high-degree ℓ modes ($\ell \geq 6$) are excited in δ Sct stars (see Figure 8 in Poretti et al. 2009 and Figure 13 in Mantegazza et al. 2012).

In order to provide a quick look at the pulsational content of the time series in the archive, we created a PDF figure with the average of the mean line profiles of the spectra and their standard deviation from the average for each target. Stars exhibiting LPVs clearly show a variable standard deviation along the average line profile, also giving hints where the largest deviations are (see Figure 2, again, for the case of HD 41641). On the contrary, time series without LPVs show a constant standard deviation. Figure 3 illustrates the clear constant behavior of the line profiles of HD 170133, an A-type star found to be constant also in the *CoRoT* photometric time series.

We used the mean line profiles not only to measure the $v \sin i$ of the stars, but also, if possible, to indicate the presence of differential rotation. This is done using the Fourier transform of the symmetrized mean line profiles, obtained by mirroring the profiles at the center and averaging the original and mirrored profiles. The position of the first zero of the transform, q_1 , is used to compute the $v \sin i$ value. The q_2/q_1 ratio of the first two zero positions is an indication of possible solar-like differential rotation (if $q_2/q_1 < 1.72$), anti-solar differential rotation (if $q_2/q_1 > 1.83$), or rigid rotation (if $1.72 < q_2/q_1 < 1.83$; Reiners & Schmitt 2002). This only works in case of rotators with $v \sin i > 10 \text{ km s}^{-1}$, where the rotation is the main contributor to the line broadening; otherwise we estimated $v \sin i$ from the FWHM of the Gaussian fitting of the mean line profiles and set the q_2/q_1 indicator as null.

The region of uncertainty around the zero positions of the Fourier transform is given by $S_f = S_p \Delta x N^{1/2}$, where S_p is the

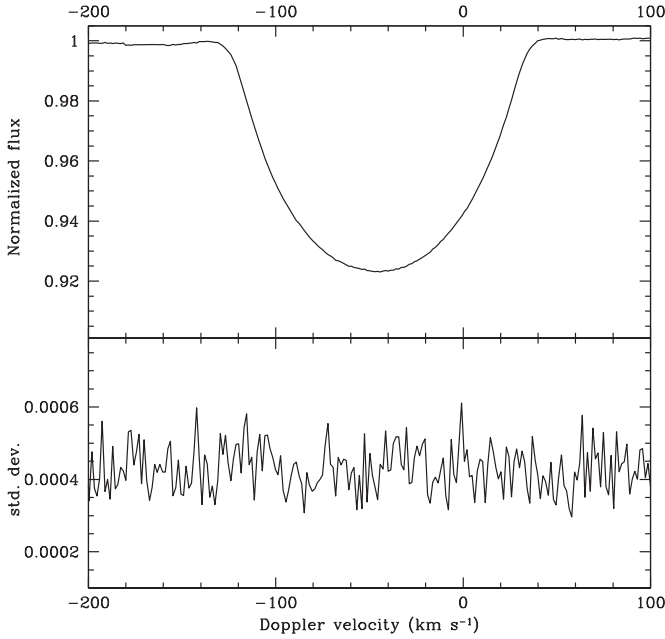


Figure 3. Average mean line profile and standard deviations for A-type star HD 170133, where no line-profile variations are present.

standard deviation between the mean line profile and its mirrored profile, Δx is the step of the data, and N is the number of data in the line profile. As such, the errors increase with the broadening of the lines and when the profiles are heavily deformed by pulsations. Then, we propagated the errors linearly to find the uncertainties on $v \sin i$ and q_2/q_1 .

As an example, we obtained $v \sin i = 77.3 \pm 0.2 \text{ km s}^{-1}$ and $q_2/q_1 = 1.80 \pm 0.01$ for a spectrum of the non-variable star HD 170133 with $S/N = 152$ (Figure 4, bottom panel). The uncertainty on the zero position is very small due to the excellent mean line profile (Figure 3). The situation is more complicated for the δ Sct variable HD 41641. Examining a spectrum with $S/N = 173$, the effects of the pulsations on the mean line profiles resulted in much larger errors, i.e., $v \sin i = 29.8 \pm 2.2 \text{ km s}^{-1}$ and $q_2/q_1 = 1.76 \pm 0.26$ (Figure 4, top panel). The indicators of differential rotation suggest rigid-body models for both stars.

We provided the radial velocities computed by the HARPS pipeline for the HAM spectra, while we computed those of the EGGs spectra by fitting the mean line profiles with a Gaussian. Indeed, it was not possible to use the simultaneous lamp calibration in the EGGs mode because the dedicated fiber was broken. Moreover, most of our EGGs targets are hotter than the masks used by the ESO pipeline to compute the cross-correlation function: as such, the radial velocity computed by the HARPS pipeline is not as accurate as in the HAM mode.

3.2. Activity Index

Our index is not calibrated on the Mount Wilson one, since it is intended to be used to study variations only, not absolute values of activity. We decided to provide an indication of the stellar activity in order to better characterize the targets and to help study the stellar variations due to the pulsations along with activity variations. Because of the large range of spectral types, we defined a simple index using the H and K lines of Ca II (Rainer et al. 2006). To do this, an automated procedure shifts the spectra by their radial-velocity values and applies a specific

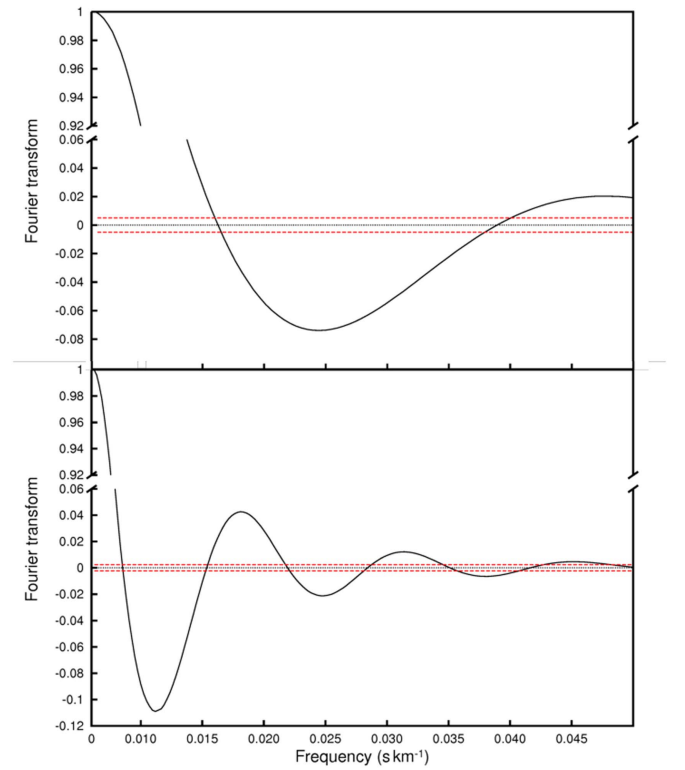


Figure 4. Top panel: Fourier transform of the mean line profile of a spectrum of the δ Sct star HD 41641 ($S/N = 173$). Bottom panel: the same for a spectrum of the non-variable star HD 170133 ($S/N = 152$). The red dashed lines show the regions of uncertainty around the zero positions.

normalization around the H and K lines. The latter step is necessary because our pipeline performs a global normalization on the whole spectrum for all different kinds of stars, and, as such, it may underestimate the continuum in the blue orders, where the S/N is usually very low, especially in the case of cool stars (see Appendix A). A simple linear interpolation using two continuum regions on the two sides of the Ca II spectral lines (3987–3918 Å and 4000–4080 Å) is enough to correct this problem. Then, the program computes the areas of four spectral regions: two regions of 2.5 Å each in the center of the H and K lines (A_H and A_K) and two regions of 10 Å each on the continuum (A_{c1} and A_{c2}).

We obtained two indices, one for the H line and one for the K line:

$$I_H = \frac{A_H}{(A_{c1} + A_{c2})/2} \quad I_K = \frac{A_K}{(A_{c1} + A_{c2})/2}. \quad (1)$$

The final index is simply the average of the two individual ones,

$$I_{HK} = \frac{I_H + I_K}{2} = \frac{A_H + A_K}{A_{c1} + A_{c2}} \quad (2)$$

Values of I_{HK} larger than 0.2–0.3 indicate the presence of activity in the specific HARPS spectrum. The index is very useful to trace activity of solar-like stars, less for hotter stars (spectral type A or earlier), but it is automatically computed and as such it is given for all the spectra. The activity index can be relied upon for more than 100 stars of our sample.

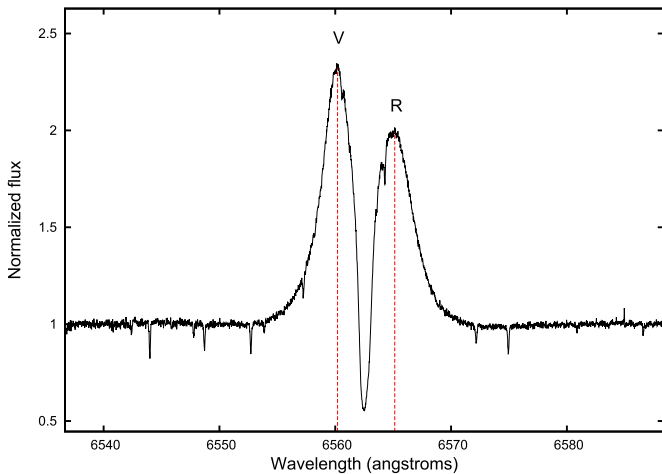


Figure 5. Observed spectrum of the Be star HD 171219 in the $H\alpha$ region. The violet and red peaks of the emission are shown with dashed lines.

3.3. Violet-to-red Peak-intensity Ratio in Be Stars

There are 40 stars in our archive that show emission lines, mostly Be stars, i.e., stars from late-O to early-A spectral types surrounded by circumstellar disks fed by stellar mass-loss outbursts: the emission lines of these stars are produced both by the stellar outbursts and by the disk.

Be stars show spectral and photometric variability on wide timescales, ranging from minutes to years; an interesting quantity to study is the violet-to-red peak-intensity ratio (V/R), which is the ratio between the peak intensity of the violet and the red part of the $H\alpha$ emission, and, as such, it is an indicator of the line asymmetry (Saad et al. 2012). Figure 5 shows the $H\alpha$ profile of the Be star HD 171219 (L. Andrade et al. 2016, in preparation). In most cases, Be stars have a stable V/R equal to 1 (no asymmetry), but roughly one-third of them show instead quasi-periodic V/R variations, which may be a combination of orbital period and long-term variability (on a timescale of several years).

All the spectra in our archive have a true/false flag for the presence of emission in the $H\alpha$ line. In the case of emission, the value of V/R is given; if there is no emission, V/R is set to zero.

4. DATA ANALYSIS: PHYSICAL PARAMETERS

The physical parameters of all the stars in the database are estimated with the spectral synthesis method using the 3.3 version of the SME software (Valenti & Piskunov 1996) and the stellar line lists from VALD (Piskunov et al. 1995) on a selected wavelength region (5160–5190 Å). We usually have several spectra for each star: in these cases, we shifted the spectra by their measured radial velocities and then averaged them, in order to lessen the effect of the pulsations on the shape of the stellar lines. We then computed the physical parameters (T_{eff} , $\log g$, and $[\text{Fe}/\text{H}]$) on the average spectrum.

To estimate their error bars, we calculated the external uncertainties, i.e., the differences between the SISMA values and those reported in papers where the detailed analyses of the *CoRoT* targets were performed. We consider these external uncertainties to be more realistic than the standard deviations of the parameters of the same star obtained from different spectra (i.e., internal uncertainties). In evaluating the external uncertainties, we have to keep in mind that both determinations are

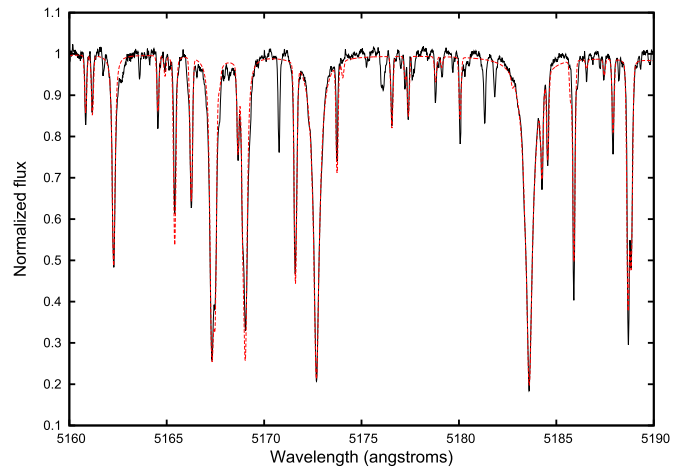


Figure 6. Observed spectrum of the δ Scuti star HD 39996 (solid black line) and best synthetic fit (red dashed line).

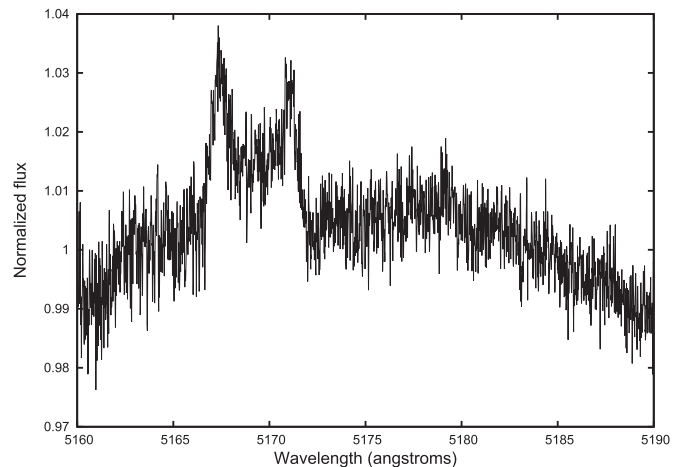


Figure 7. Observed spectrum of the Be star HD 128293 in the 5160–5190 Å region. The emissions are clearly visible. It is not possible to fit this spectrum in order to estimate the physical parameters of the star.

affected by their own error bars and we are comparing a single method to several different case-by-case ones. Using a sample of 25 stars, we obtained mean differences of 240 K (i.e., 4.0%) in T_{eff} , 0.32 dex in $\log g$, and 0.33 dex in $[\text{Fe}/\text{H}]$ for cool ($T_{\text{eff}} < 6000$ K) main sequence stars. These values are very close to the external uncertainties obtained from the LAMOST parameters and the literature ones: 3.5%, 0.3 dex, and 0.2 dex (Frasca et al. 2016). The uncertainties increase to 400 K in T_{eff} , 0.50 dex in $\log g$, and 0.40 dex in $[\text{Fe}/\text{H}]$ when extending the sample to early-type stars, as expected by including very fast rotators, such as B-type stars. Indeed, their parameters are strongly method-dependent due to line blending and their almost-complete dilution in the continuum.

To allow the user to have an immediate feeling of the strength of the given set of the parameters, we also provide for each star a PDF figure with the observed spectrum and the best fit (Figure 6). Under very special circumstances (e.g., very fast rotators, emission-line stars, binary stars, and so on), we were not able to estimate the physical parameters with this automated method, e.g., in the specific case of the strong emission lines of the Be star HD 128293 (Figure 7). In these cases, a PDF figure with only the observed spectrum in the 5160–5190 Å region is given in the archive.

Table 2

Spectroscopic Information On the Observed Targets: Number of Spectra and Their S/N Range, Physical Parameters, Variability Type, Binarity and Emission Flags

Target Name	Number of Spectra	T_{eff} (K)	$\log g$ (cgs)	[Fe/H]	Binary Flag	Variable Type	H α Emission	S/N Range
BD 184914	1	7162	3.21	0.43	no	dSct	no	93
GSC 00144-03031	3	7822	3.41	0.09	no	dSct	no	109–121
HD 001097	1	6595	3.70	0.31	no	dSct	no	123
HD 007312	1	8378	3.88	0.55	no	dSct	no	216
HD 008781	1	7280	2.91	−0.23	no	dSct	no	132
HD 009065	35	7471	3.30	−0.41	no	dSct	no	129–378
HD 009133	1	8812	4.25	0.49	no	dSct	no	117
HD 010167	1	SB2	gDor	no	265
HD 011462	10	11891	4.05	0.07	no	bCep	no	74–194
HD 011956	1	8986	3.93	0.71	no	dSct	no	197
HD 016031	14	5633	4.38	0.13	no	no	no	57–89
HD 016189	65	7338	3.72	0.00	no	dSct	no	131–419

(This table is available in its entirety in machine-readable form.)

Finally, we made available online a table with the estimated physical parameters and other information (variability type, binarity, and so on). A portion is shown in Table 2.

5. CoRoT PHOTOMETRY

The most observed stars, i.e., those with more spectra in the archive, are the main asteroseismic targets of the *CoRoT* Long Runs. In fact, the ground-based campaigns were planned to have the spectroscopic counterpart of the *CoRoT* light curve. The light curves of these 72 stars have been retrieved from the *CoRoT* public archive and stored in our database alongside the spectra. In some cases, the targets were observed with *CoRoT* in more than a Long Run, resulting in more than one set of photometric data per target. The *CoRoT* data are the legacy light curves (Baglin et al. 2016).⁷

The light curves are provided as FITS files, with some auxiliary information stored in the header. The FITS files contain three tables: RAW (N1 data with correction from aliasing, offsets, background and satellite’s jitter), BAR (N2 data with some flux correction for thermal effects and long term efficiency, and spurious points replaced by interpolation), and BARREG (BAR N2 data with invalid and missing data replaced using the Inpainting method; Pires et al. 2015).

The nights with HARPS were scheduled during the period of best visibility of the *CoRoT* targets, and we were usually able to get the requested simultaneous spectroscopy and photometry. However, the time baseline of the spectroscopic observations is much smaller than that of the photometric ones (typically 20–25 nights against 30–150 days). Nevertheless, it was possible to monitor the spectroscopic counterpart of the photometric variations: Figure 8 shows an example of simultaneous radial-velocity and flux measurements.

6. CONCLUSIONS

With the large number of space missions and ground-based campaigns that are continuously carried on, it becomes important to store the large amount of observational data in an easily accessible database so that it can be exploited by the whole scientific community, both to re-analyze the available

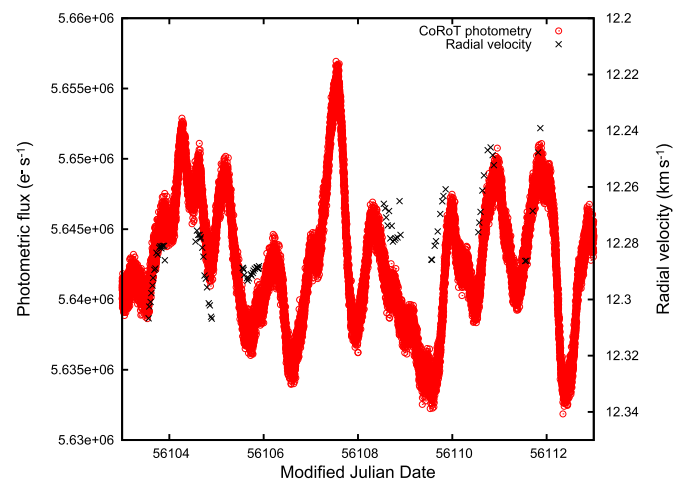


Figure 8. Zoom of the simultaneous plot of the *CoRoT* light curve (red dots) and the radial-velocity curve (black crosses) of the red giant HD 178484. Instead of the radial velocities, it is possible to plot any of the other spectroscopic indicators, i.e. $v \sin i$, q_2/q_1 , activity indices, or V/R values.

data with different tools and to help in the preparation of future missions and related archives.

The ground-based spectra played a key role in the exploitation of the *CoRoT* mission thanks to the coordinated starting of the spectroscopic and photometric campaigns. Toward this goal, we built the online database SISMA using the high-resolution HARPS spectra observed simultaneously with the *CoRoT* satellite and the relative light curves. While the *CoRoT* targets, with their simultaneous spectroscopy and photometry, are the backbone of the archive, we would like to highlight the importance of the many non-*CoRoT* targets, aimed at improving the study of classes of variable stars by means of the provided indicators, for the most part still unpublished and unused in a statistical sense. The high S/N, high-resolution, fully reduced and calibrated archival spectra are enriched with many observational parameters to be directly used as tools to investigate the spectroscopical effects of the stellar variability: mean line profiles, differential rotation indicators, activity indices, H α violet-to-red peak-intensity ratio, along with the computed $v \sin i$ and radial-velocity values. In addition to that, the stellar atmospheric parameters

⁷ http://www.edp-open.org/index.php?option=com_content&view=article&id=317

available in the archive are computed in an homogeneous way. The structure of the archive is explained in the Appendix B.

The SISMA archive offers the possibility to study the stellar variability from different perspectives. To give a few examples, (i) the interplay between rotation rate and distribution of pulsational frequencies in hot variables close to the main sequence. The link between rotational frequencies, large separations, and regular spacings is a promising topic in the study of δ Sct stars (García Hernández et al. 2015; Páparó et al. 2016) and γ Dor stars (Van Reeth et al. 2016); (ii) the presence of circumstellar, narrow emission structures in the core of absorption lines of fast rotators indicating the rate occurrence of mass-loss events; (iii) the relation between activity indices and differential rotation in cool stars, a very useful tool to investigate star–planet interactions (Borsa et al. 2015).

We feel that the SISMA database fully matches the need to provide a set of high-quality data to be used beyond the asteroseismic community that planned the observations and to be used for purposes much wider than those driving them at the beginning of the *CoRoT* adventure.

This work is based on observations made with the 3.6 m telescope at La Silla Observatory under the ESO Large Programmes LP182.D-0356 and LP185.D-0056. The research leading to this result has received funding from the European Community’s Seventh Framework Programme ([FP7/2007-2013]) under grant agreement No. 312844. The authors thank Artie Hatzes for useful comments on a first draft of the manuscript.

Facilities: ESO:3.6m (HARPS spectrograph), *CoRoT*.

Software: LSD (Donati et al. 1997), SME (Valenti & Piskunov 1996), VALD (Piskunov et al. 1995), HARPS DRS, RGraph, STIL.

APPENDIX A THE REDUCTION OF THE HARPS SPECTRA

The HARPS Data Reduction Software pipeline (DRS) automatically reduces all of the observed spectra by doing bias subtraction, masking of bad columns, dark subtraction, flat-fielding, extraction of the orders, removal of the blaze function, wavelength calibration, merging of the orders, and radial-velocity computation. The final results are the merged monodimensional **s1d** files, but we were dissatisfied with the blaze removal and felt that the merging procedure resulted in loss of information on the quality of some spectral regions.

Our reduction pipeline worked with the **e2ds** FITS files given by the online DRS, i.e., the bi-dimensional spectra with the echelle orders extracted and corrected for the flat-field. These first steps are done quite well by the online pipeline, so there was no need to re-do them. Because one of our goals was to easier normalize the spectra, we took particular care in removing the blaze function from the orders. In order to do this, we observed every night a very bright hot star (HD 34816, spectral type B0.5, or HD 135240, spectral type O8, according to their visibility): because of their few spectral lines, we could easily fit their continuum and use it as the blaze function.

We also computed the S/N ratio of the spectra for each pixel by using the expression

$$S/N = \frac{1}{\sqrt{\epsilon_{\text{spectrum}}^2 + \epsilon_{\text{flat}}^2}}, \quad (3)$$

where $\epsilon_{\text{spectrum,flat}}$ is given by

$$\epsilon_{\text{spectrum,flat}} = \frac{\sqrt{\text{RON}^2 + \text{gain} \times N_{\text{spectrum,flat}}}}{\text{gain} \times N_{\text{spectrum,flat}}}, \quad (4)$$

where the read-out-noise RON is $4.5 e^-$, the gain is $0.75 \text{ ADU}/e^-$, and $N_{\text{spectrum,flat}}$ is the counts per pixel in the science and flat-field spectra, respectively. This allows us to study the spectra in detail keeping in mind the reliability of each part of the spectra.

Then, we divided the spectra for the blaze function, calibrated them in wavelength, corrected them for their barycentric velocity, and rebinned them with a 0.1 \AA step. Afterwards, we normalized the spectra in an automated way. Our pipeline normalized each order with an iterative procedure using a second-degree polynomial computed from a fixed point λ_0 chosen in the middle of the order, far from the borders:

1. our pipeline computed a first polynomial fit;
2. our pipeline computed the residuals between the spectrum and the polynomial, all of the pixels with a residual larger than 3σ are considered spectral lines, along with their adjacent pixels until the sign of the residuals changes;
3. our pipeline computed another fit on the spectrum minus the spectral lines; and
4. our procedure iterated until it converged.

Some orders may have a lot of spectral lines, in which case the normalization could be incorrect. To remedy this situation, our pipeline confronted the polynomial coefficients found for all the orders, which should be very similar in case of a correct normalization. If they differed a lot (which happened only for a couple of orders at worst), the incorrect polynomial coefficients were substituted by fitting the coefficients found for all of the spectral orders. Unfortunately, several adjacent blue orders of the spectra have this problem, worsened by the lower S/N ratio in these regions due to the efficiency of the CCD, this translates to an underestimation of the continuum in the first blue orders of the spectra.

The merging of the orders was done on the overlapping continuum regions of the normalized spectra. The pixels are weighted using their S/N ratio and averages. As such, our procedure outputted two-column normalized merged spectra (wavelength and normalized flux) and five-column normalized and un-normalized unmerged spectra (wavelength, flux, normalized flux, S/N, and echelle orders).

APPENDIX B ENSEMBLE OF THE STELLAR PARAMETERS AND STRUCTURE OF THE ARCHIVE

All of the data (reduced spectra, indicators, and photometric series) are stored as either FITS or PDF files in the SISMA archive and can be accessed at <http://sisma.brera.inaf.it/>. The data can also be accessed through the Seismic Plus portal⁸, developed in the framework of the *SpaceInn* project in order to gather and help coordinated access to several different solar and stellar seismic data sources.

⁸ <http://voparis-spaceinn.obspm.fr/seismic-plus/>

B.1. Database Infrastructure

The operating system for the online archive (database and web pages) is Linux, assembled under the model of free and open-source software development and distribution. The object-relational database management system (ORDBMS) is PostgreSQL, a free and open-source software developed by the PostgreSQL Global Development Group. The ORDBMS manages all data and files stored in the archive.

The web user interface to the database is programmed using the Java/Servlet/JSP language, that creates web-based applications using Model View Controller. The web pages are Java Server Pages (JSPs) with embedded Java, HTML, and CSS codes. The codes are executed on the server, then the page is returned to the browser for display. The server for Java Servlet and JSPs technologies is Apache Tomcat.

JSPs use RGraph⁹ for charts visualization, a JavaScript charts library that produces the charts dynamically with JavaScript and the HTML canvas tag. The charts are made inside the browser with JavaScript, so they are both quick to create and small. The archive can be queried either by target (using the name resolver service Sesame¹⁰) or by variability class, and the data can be retrieved or displayed. In the latter case, it is possible to plot the spectra, the light curves, and the spectroscopic time series online. The library used to read the FITS files is STIL (Starlink Tables Infrastructure Library).¹¹

B.2. Scientific Data

The database contains several files for each observed object:

1. *_full.fits: the main deliverables, i.e., the reduced spectra. The five-column list wavelength (barycentric corrected, in Å), reduced flux, normalized flux, S/N, and echelle order;
2. *_nor.fits: additional reduced spectra, automatically normalized and with the orders merged. They have two columns (barycentric-corrected wavelength in Å and normalized flux). It is important to keep in mind that the normalization is done by an automated procedure and, as such, a careful check is necessary for a detailed study of any particular line;
3. *_mean.fits: the mean line profiles of each spectrum computed with the LSD software in the 4415–4805, 4915–5285, and 5365–6505 Å wavelength ranges. The files consist of two columns: Doppler velocity and normalized flux;
4. OBJECT_tbl.fits: a general overview of the object time series:
 - (i) the root names of the spectra,
 - (ii) the barycentric Julian dates at mid-exposure,
 - (iii) the S/N of the spectra in the 5805–5825 Å region,
 - (iv) the radial velocities of the spectra and their errors,
 - (v) the projected rotational velocities $v \sin i$ of the spectra and their errors,
 - (vi) the q_2/q_1 values and their errors,
 - (vii) the activity index I_H , using only the Ca II H line, of each spectrum,
 - (viii) the activity index I_K , using only the Ca II K line, of each spectrum,
 - (ix) the averaged activity index I_{HK} of each spectrum,
 - (x) the H α violet-to-red peak-intensity ratio (V/R) of each spectrum,
 - (xi) in the case of double or multiple systems, the radial velocities, $v_{\sin i}$ and their errors will be listed for all the components, if possible;
5. OBJECT_profmed.pdf: a PDF file that allows a quick look at the line-profile variations of the time series. In the case of objects where a single spectrum was observed, the mean line profile of the spectrum is given instead;
6. OBJECT_fit.pdf: a PDF file with the observed spectrum in the 5160–5190 Å region and the best-fit synthetic spectrum. In the case of objects where the fit was not possible, only the observed spectrum is given.
7. CoRoT light curves: FITS files with the CoRoT photometry. The light curves are available only for the 72 CoRoT targets having at least one HARPS spectrum.

To summarize, SISMA contains reduced photometric and spectroscopic observations and time series of spectroscopic indicators. The physical parameters of the stars and the various indices are properly stored also in the FITS headers of the reduced spectra.

REFERENCES

- Baglin, A., Auvergne, M., Barge, P., et al. 2007, *AIPC*, **895**, 201
- Baglin, A. & the CoRoT team 2016, The CoRoT Legacy Book: The adventure of the ultra high precision photometry from space (Les Ulis: EDP Sciences)
- Blomme, R., Briquet, M., Degroote, P., et al. 2012, *ASPC*, **465**, 13
- Borsa, F., Scandariato, G., Rainer, M., et al. 2015, *A&A*, **578**, A64
- Donati, J.-F., Semel, M., Carter, B. D., Rees, D. E., & Collier Cameron, A. 1997, *MNRAS*, **291**, 658
- Escorza, A., Zwintz, K., Tkachenko, A., et al. 2016, *A&A*, **588**, A71
- Floquet, M., Hubert, A.-M., Huat, A. L., et al. 2009, *A&A*, **506**, 103
- Frasca, A., Molenda-Zakowicz, J., De Cat, P., et al. 2016, *A&A*, **594**, A39
- García Hernández, A., Martín-Ruiz, S., Monteiro, M. J. P. F. G., et al. 2015, *ApJL*, **811**, L29
- Gkouvelis, L., Fabregat, J., Zorec, J., et al. 2016, *A&A*, **591**, A140
- Mantegazza, L., Poretti, E., Michel, E., et al. 2012, *A&A*, **542**, A24
- Mayor, M., Pepe, F., Queloz, D., et al. 2003, *Msngr*, **114**, 20
- Paparo, M., Benkő, J. M., Hareter, M., & Guzik, J. A. 2016, *ApJS*, **224**, 41
- Pires, S., Mathur, S., García, R., et al. 2015, *A&A*, **574**, A18
- Piskunov, N., Kupka, F., Ryabchikova, T. A., Weiss, W. W., & Jeffery, C. S. 1995, *A&AS*, **112**, 525
- Poretti, E., Michel, E., Garrido, R., et al. 2009, *A&A*, **506**, 85
- Poretti, E., Rainer, M., Mantegazza, L., et al. 2013, *ASSP*, **31**, 39
- Poretti, E., Rainer, M., Uytterhoeven, K., et al. 2007, *MmSAIt*, **78**, 624
- Poretti, E., Rainer, M., Weiss, W. W., et al. 2011, *A&A*, **528**, A147
- Rainer, M. 2003, Laurea thesis, Univ. degli Studi di Milano
- Rainer, M., Bossi, M., & Mantegazza, L. 2006, *ASPC*, **349**, 319
- Rainer, M., Poretti, E., Mathias, P., et al. 2012, *AN*, **333**, 1061
- Reiners, A., & Schmitt, J. H. M. M. 2002, *A&A*, **384**, 155
- Saad, S. M., Hamdy, M. A., & Abolazm, M. S. 2012, *JAsGe*, **1**, 97
- Uytterhoeven, K., Poretti, E., Mathias, P., et al. 2009, *AIPC*, **1170**, 327
- Valenti, J. A., & Piskunov, N. 1996, *A&AS*, **118**, 595
- Van Reeth, T., Tkachenko, A., & Aerts, C. 2016, *A&A*, **593**, 120

⁹ <http://www.rgraph.net/>

¹⁰ <http://cdsweb.u-strasbg.fr/doc/sesame.thx>

¹¹ <http://www.star.bristol.ac.uk/~mbt/stil/>